VTT Technical Research Centre of Finland

On the Optimum Propeller Loading with Inclusion of Duct and Hub

Sanchez Caja, Antonio

Published in:
Transactions of the Royal Institution of Naval Architects, RINA

Published: 01/01/1991

Document Version
Peer reviewed version

THE ROYAL INSTITUTION OF NAVAL ARCHITECTS

ISSUED FOR WRITTEN DISCUSSION **W7 (1990)**

Contributions to the discussion of this paper are invited; they should be typewritten and should reach the Secretary, The Royal Institution of Naval Architects, 10 Upper Belgrave Street, London SW1X 8BQ not later than January 11, 1990.

The Institution is not, as a body, responsible for the statements made nor for the opinions expressed by individual authors.

ON THE OPTIMUM PROPELLER LOADING WITH INCLUSION OF DUCT AND HUB

by A. Sánchez*

SUMMARY: A numerical approach to determine the optimum circulation of a propeller operating inside a duct and hub is presented. The procedure combines a potential-based panel method for treating the flow around the duct and hub surfaces, and a vortex lattice lifting line method for treating the propeller.
The optimum propeller loading is determined by using a non-linear optimization technique to maximize the propeller efficiency. The non-axisymmetric interactions between the duct-hub surface and the propeller are considered within the design procedure. Optimum results for a propeller operating independently with either a duct or a hub are included.

1. INTRODUCTION

Ducted propellers have been used during the last few decades on a broad extent of ship applications which range from large commercial ships to naval destroyers. General reasons for these installations include higher propulsor efficiency, smaller propeller size, improved blade loading, controlled flow through the propeller and consequently reduction of cavitation as well as of propeller excited vibration, protection of the propeller from damage, etc.

The greater part of the research to obtain a reliable analytical method for the design and hydrodynamic analysis of ducted propellers has focused on the axisymmetric problem of a duct interacting with an actuator disk, in other words, with an infinite-bladed lifting line. The earliest representations of a duct were fully linearized, with singularities representing the duct thickness and loading projected onto a mean cylindrical surface. Morgan [15] and Caster [1] are representative of this stage of the ducted propeller theory.

The next generation of analysis methods represented the duct in a non-linear theory, first placing the singularities on geometrically more complicated surfaces, and finally, on the actual surface. The work of Gibson and Lewis [3] and of Glover and Ryan [4] are contributions in that area.

With respect to the interaction between blades and hub, the first analysis methods represented the hub as an infinitely long cylinder with two boundary conditions, namely, the circulation and the radial velocity component are both zero at the hub. The work of Lerbs [11] is representative of this stage.

McCormick [13] extended Goldstein's [5] hubless solution to include a hub with nonzero radius and infinite length. He formulated the potential problem for a lightly loaded lifting line with vanishing normal velocity conditions on the hub and on the trailers. The solution for the velocity potential was an infinite series of modified Bessel functions and Lommel's function. He found that the circulation was nonzero at the hub. The slope of the circulation at the hub was almost zero in his results, although this was not pointed out in his paper.

Kerwin and Leopold [8] studied the non-axisymmetric flow induced by lifting lines operating in the presence of a hub using a vortex lattice model to represent the trailing vortices. They assumed that the slope of the bound circulation at the hub was zero and used an image system with vortices inside the hub to satisfy the normal velocity boundary conditions on the hub surface. This was based on the assumption that two-dimensional vortex image theory is approximately valid for the three-dimensional case provided that the pitch angle is sufficiently high. They showed that this approximation was good for vortices near the hub, but not for the distant elements.

Recently, Ludolph [12] represented the hub by a series of ring sources, Hess and Valarezo [6] used a surface panel method to model the propeller, with source and dipole panels representing the blade and source panels for the hub.

Wang [14] developed an iterative method for analyzing the interference between the blades and the hub using vortex rings to represent the hub, and chordwise vortex lattice and spanwise source lattice to represent the camber surfaces of the blades. He has shown that the increase in thrust due to hub effects has the same order of magnitude as the drag force effects on the hub for propellers which are moderately loaded at the hub.

More recently Lee [10] used sources and dipoles to model both the blades and the hub. He showed that a lower panel method based on the perturbation potential is robust for treating extreme geometries and requires a relatively small computational effort.

On the other hand, very recently Kerwin, Kinnas, et al. [7] have developed a method for the analysis of ducted propellers which combines a potential based method for the flow on the duct with a lifting surface method for the flow on the propeller. The strong angular variation of circulation and pressure distributions around the duct obtained in their work suggests that the non-axisymmetric interactions between the propeller and other control surfaces should be considered in the first stages of a design procedure.

The design of ducted propeller has usually been achieved by a trial and error procedure. To avoid such an approach, a method

*Naval Architect
SENERMAR, Madrid, Spain

which combines a systematic way to determine the optimum propeller loading and a non-linear representation of the duct and hub, is desired. Such a method using a lifting line representation of the propeller and a panel method representation of the duct, has been developed by Kinnas and Coney [9].

In the present work their approach has been extended to include a panel method representation of the hub. The neglect of the hub could be justifiable from the standpoint of overall propeller performance because of the small contribution of the blade to overall propeller forces in the immediate vicinity of the hub. However, the solution for the circulation distribution is incorrect in this region.

A computer program has been developed to handle independently, combinations of:
* duct, hub, and lifting lines
* duct and lifting lines
* hub and lifting lines,

and to obtain optimum distributions of circulation and other hydrodynamic parameters of interest such as chordlength distribution on the propeller, pressure distributions on duct and hub, etc. In the two cases where the geometry of the hub is involved, nonzero values of circulation at the root of the blade are illustrated.

2. THEORETICAL FOUNDATIONS

2.1 STATEMENT OF THE PROBLEM

Consider a closed three dimensional fluid domain V with boundary S and the unit normal vector $\mathbf{n}$ to S oriented into V as shown in Figure 1, taken from reference 10. The boundary S is composed of the duct and hub surface S_B, the wake surface S_W, and the outer control surface S_∞ surrounding the fluid domain. The body is subject to an inflow velocity $\mathbf{U}_{inflow}$. If the fluid on V is assumed to be incompressible, inviscid, and irrotational, there exists a perturbation velocity potential ϕ which satisfies the Laplace equation and which is defined as

$$\nabla\phi = \vec{q} - \vec{U}_{inflow} \tag{1}$$

where $\mathbf{U}_{inflow}$ is the incoming velocity and $\mathbf{q}$ is the total velocity at any point in the fluid. A boundary-value problem can be constructed with the following boundary conditions:

* The *kinematic boundary condition* must be satisfied at each point q on S_B,

$$\frac{\partial\phi}{\partial n_q} = -\vec{U}_{inflow}\cdot\vec{n}_q \tag{2}$$

* A *Kutta condition* is required at the trailing edge of the duct: the velocity must be finite.

* The wake surface of the duct (S_W) is assumed to have zero thickness. The normal velocity jump across this surface is zero, while a jump on the potential is allowed.

$$\begin{aligned}\left(\Delta\frac{\partial\phi}{\partial n_q}\right)_{S_W} &= 0\\ (\Delta\phi)_{S_W} &= \phi^+ - \phi^- = \Gamma\end{aligned} \tag{3}$$

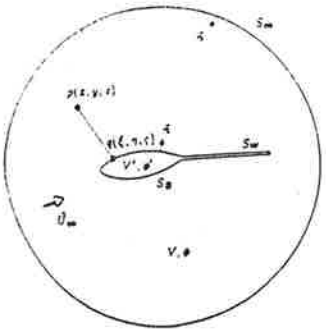

Fig. 1: Notation for the application of Green's theorem

* On the outer control surface the perturbation velocity due to the body should vanish.

Applying Green's theorem we can find the perturbation potential at any field point p in the fluid as a function of the value of the perturbation potential at the points q on the surface S. In particular if the field point is located on the duct-hub surface S_B,

$$2\pi\phi(p) = \iint_{q\in S_B}\left[\phi(q)\frac{\partial}{\partial n_q}\left(\frac{1}{R(p,q)}\right) - \frac{\partial\phi(q)}{\partial n_q}\frac{1}{R(p,q)}\right]dS + \iint_{q\in S_W}\Delta\phi(q)\frac{\partial}{\partial n_q}\frac{1}{R(p,q)}dS \tag{4}$$

where p is a field point on S_B, q is a point on S_B and S_W, $R(p,q)$ is the distance between points p and q, and $\Delta\phi$ is the jump of the potential on S_W.

Equation (4) is a Fredholm integral of the second kind with respect to the unknown potential $\phi(p)$ and can be discretized by approximating the duct-hub surface, and the trailing wake with quadrilateral panels. Then it can be solved for the unknown potential by applying it at a set of appropriate control points. The strength of the sources in equation (4) is given by equation (2) and that of the dipoles in the wake is given by the difference of the potentials at the upper and lower panels of the duct trailing edge as suggested by Morino [16]. The singularity densities are approximated by constant distributions on each panel.

Accounting for Hub, Duct, and Lifting Lines

To apply the general panel method in the case of lifting lines operating inside a duct and hub, the following correspondences have been made:

* S_B is the surface of the hub including the hub vortex plus that of the duct. The hub together with the blades will be modelled by source and dipole panels as described by Lee [10].
* S_W now includes not only the wake surface of the duct, S_{Wd} but also that of the lifting lines, S_{WL}.

The potential on the duct-hub panels due to the lifting lines has been evaluated following a panel method pattern. The lifting lines can be considered as singular actuator lines which produce a difference of potential between the sides of their wake. This difference of potential is mantained constant along each infinitesimal helical wake strip shed from the

lifting lines. The local circulation at each point, l, of the lifting lines gives the value of the local difference of potential for each infinitesimal helical strip on the wake. Therefore,

$$[\Delta\phi(l)]_{S_{WII}} = \Gamma(l),$$

and equation (4) becomes

$$2\pi\phi(p) = \iint_{q\in S_B}\left[\phi(q)\frac{\partial}{\partial n_q}\left(\frac{1}{R(p,q)}\right) - \frac{\partial\phi(q)}{\partial n_q}\frac{1}{R(p,q)}\right]dS + \iint_{q\in S_{WI}}\Delta\phi(q)\frac{\partial}{\partial n_q}\frac{1}{R(p,q)}dS - 4\pi\phi_{LL}(p), \quad (5)$$

where ϕ_{LL} can be defined as the potential due to the lifting lines and can be expressed as

$$-4\pi\phi_{LL}(p) = \iint_{q\in S_{WII}}\Delta\phi(l)\frac{\partial}{\partial n_q}\frac{1}{R(p,q)}dS. \quad (6)$$

Notice that in equation (6) the points q on the lifting line wake and l on the lifting line are placed on the same infinitesimal helical strip of the wake. In a discrete lifting line model, they will both lie on the same horseshoe.

2.2 DUCT, HUB, AND PROPELLER INTERACTIONS

In order to determine the influence of the duct and hub surfaces on the distribution of thrust and torque along the propeller lifting lines, it will first be necessary to analyze the components of the velocity field.

The inflow at the lifting lines will be considered as the linear superposition of the axisymmetric flow along the duct and hub surfaces, plus the one generated by the lifting lines acting alone, plus that due to the interaction of the duct-hub surface and the lifting lines. This last flow is found by first determining the potential induced on the duct and hub surface due to the lifting lines and then by computing the velocities due to this potential.

Therefore, the total velocity with respect to a propeller frame rotating with angular velocity w can be decomposed, at any control point l of the lifting line, into four components:

$$\vec{q}(l) = \vec{U}_{inflow}(l) + \vec{q}_0(l) + \sum_{i=1}^{m}\Gamma_i\vec{q}_i(l) + \vec{q}_{LL}(l) \quad (7)$$

where
* U_{inflow} is the free stream velocity (U_∞) plus the circumferential velocity (w x r) at any point l located at a distance r from the axis of rotation
* q_0, the velocity due to the interaction between the incoming flow (U_{inflow}) and the duct-hub surface
* q_i, the velocity due to the interaction between duct-hub and the ith unit strength horseshoe
* q_{LL}, the velocity induced by the lifting lines.

The last three components can be expressed in terms of their perturbation potentials ϕ_0, ϕ_i, and ϕ_{LL} respectively.

The potential induced by the lifting lines can be linearly decomposed as follows

$$\phi_{LL} = \sum_{i=1}^{m}\Gamma_i\phi_{LL,i} \quad (8)$$

where Γ_i is the strength of the ith horseshoe and $\phi_{LL,i}$ is the potential induced by the ith unit strength horseshoe. This will also be true for points located on the duct-hub surface. Therefore, if p is a point on S_B,

$$\phi_{LL}(p) = \sum_{i=1}^{m}\Gamma_i\phi_{LL,i}(p)$$

On the other hand, the perturbation potential on S_B can be expressed as

$$\phi(p) = \phi_0(p) + \sum_{i=1}^{m}\Gamma_i\phi_i(p) \quad (9)$$

where $\phi_i(p)$ is the potential on S_B due to the interaction between S_B and the ith unit strength horseshoe, and $\phi_0(p)$ is the perturbation potential due to an axisymmetric flow on S_B without lifting line effects.

Note that ϕ_i and $\phi_{LL,i}$ are related by Green's theorem:

$$2\pi\phi_i(p) = \iint_{q\in S_B}\phi_i(q)\frac{\partial}{\partial n_q}\frac{1}{R(p,q)}dS + \iint_{q\in S_W}\Delta\phi_i(q)\frac{\partial}{\partial n_q}\frac{1}{R(p,q)}dS - 4\pi\phi_{LL,i}(p). \quad (10)$$

The integral over S_B lacks the source term since no inflow is present in this case. Note also that ϕ_0 must satisfy the equation

$$2\pi\phi_0(p) = \iint_{q\in S_B}\left[\phi_0(q)\frac{\partial}{\partial n_q}\frac{1}{R(p,q)} + [\vec{U}_{inflow}\vec{n}_q]\frac{1}{R(p,q)}\right]dS + \iint_{q\in S_W}\Delta\phi_0(q)\frac{\partial}{\partial n_q}\frac{1}{R(p,q)}dS \quad (11)$$

2.3 COMPUTATION OF PRESSURE DISTRIBUTIONS

As developed in Appendix C of Ref. 7, once the potential on the duct and hub surfaces is known, the total velocity **q** with respect to the rotating system is determined as

$$\mathbf{q} = \mathbf{U}_E + \nabla\phi \quad (12)$$

where $\mathbf{U}_E$ is the relative effective incoming velocity and $\nabla\phi$ is the perturbation velocity at the point under consideration. In turn, the relative incoming inflow can be represented as

$$\mathbf{U}_E = \mathbf{w} \times \mathbf{r} + \mathbf{U}_\infty \quad (13)$$

and the perturbation velocity, as

$$\nabla\phi = \nabla_n\phi + \nabla_s\phi \quad (14)$$

where **w** is the vorticity of the fluid with respect to the rotating system, **r** is the vector distance from the axis of rotation, $\mathbf{U}_\infty$ is the axial inflow velocity, $\nabla_n\phi$ is the component of the perturbation velocity normal to the body surface and can be obtained from equation (2), and $\nabla_s\phi$ is the component of the perturbation velocity tangent to the body surface.

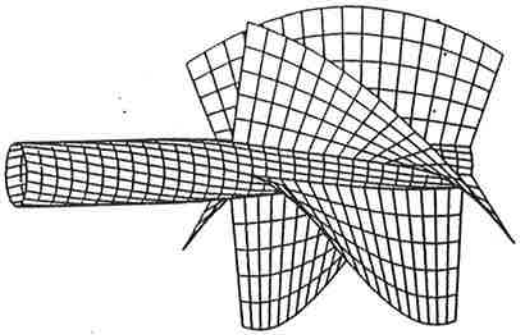

Figure 2: Panel arrangement on a hub and on the wakes of five equally spaced lifting lines. The lifting lines are modelled as five horseshoes of equal span.

Then the pressure distribution is found by applying Bernoulli's equation along a streamline in the absolute system

$$p_\infty/\rho + U_\infty^2/2 = p/\rho + [q^2 - (\Omega \times r)^2] \qquad (15)$$

where p is the pressure at a point on the surface, p_∞ is the pressure further upstream on the same stream surface, ρ is the fluid density and Ω is the propeller angular velocity.

The pressure is finally expressed in terms of the pressure coefficient C_p, which is defined as

$$C_p = (p - p_\infty)/0.5\ \rho\ U_\infty^2 \qquad (16)$$

By combining equations (15) and (16),

$$C_p = 1 - [q^2 - (\Omega \times r)^2]/\ U_\infty^2 \qquad (17)$$

The force on the duct is computed by summing the pressure forces on each panel.

The force on the hub is not accounted for in the present optimization scheme. This is a limitation of the current work since a large circulation at the hub would result in large hub vortex drag.

2.4 VORTEX LATTICE LIFTING LINE MODEL

The assumptions which have been adopted in the lifting line model are as follows:

* the propeller blades are represented by straight, radial lifting lines, with equal angular spacing and identical loading
* the wake geometry is assumed to be helical with a pitch at each radius determined by the undisturbed inflow at the lifting line (linear theory) or by the induced flow at the lifting line (moderately loaded theory)
* the continuous distribution of vortices along the lifting line is discretized as a lattice of concentrated straight-line elements of constant strength.

The element arrangement in this work uses constant spacing. In the cases where either the hub or the duct is combined with the lifting lines independently, one quarter inset is employed at the endpoint of the lifting lines in contact with the fluid

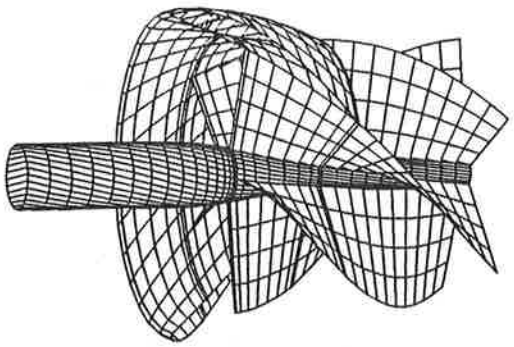

Figure 3: Panel arrangement on a duct, on a hub and on the wake of five equally spaced lifting lines. The lifting lines are modelled as three horseshoes of equal span.

in order to represent properly the square root singularity at the tip. This will occur either at the outer endpoint of the lifting lines, in the case in which only hub and lifting lines are studied, or at the inner endpoint, in the case in which only the duct is combined with the lifting lines. When the lifting lines are operating inside both duct and hub, no inset is used because no gap is accounted for in this work.

Figures 2 and 3 show the panel arrangements on the wakes behind the lifting lines for both a combination of hub and lifting line and a combination of duct, hub, and lifting lines. The paneling on the duct and hub will be explained in more detail in the following Section.

2.4.1 FORCE CALCULATIONS

The force acting at a radius r on the lifting line is derived from local application of Kutta-Joukowski's law. The axial and tangential induced velocities combine with the nominal inflow to produce an effective inflow $V(r)$ directed at an angle $\beta_i(r)$ with respect to the plane of rotation. A force per unit radius

$$F(r) = \rho V^*(r)\Gamma(r) \qquad (18)$$

is directed at right angles to $V^*(r)$. The effect of viscous drag is included by adding a force $F_v(r)$ acting in a direction parallel to V^*. This force is estimated on the basis of an experimentally determined two-dimensional sectional drag coefficient, $C_D(r)$. This means that the section chordlength $l(r)$, must be specified.

The resultant force may then be resolved into axial and tangential components

$$\begin{aligned} F_z(r) &= \rho V^*(r)\cos\beta_i(r) - (1/2)\rho\,(V^*(r))^2\, l(r) C_D(r)\sin\beta_i(r) \\ F_t(r) &= \rho V^*(r)\sin\beta_i(r) + (1/2)\rho\,(V^*(r))^2\, l(r) C_D(r)\cos\beta_i(r) \end{aligned} \qquad (19)$$

2.4.2 VARIATIONAL OPTIMIZATION

With the variational optimization we try to find, for a discrete model, the optimum distribution of circulation given the propeller's operating conditions; in other words, the

radial distribution of circulation which provides a prescribed total thrust, T_T, for a minimum torque, Q. The total thrust has two components: thrust generated by the propeller, T_P, and thrust generated by the duct, T_D.

Under the discrete model used in the optimization scheme the forces on the propeller become, as developed in Ref. 2:

$$T_P = \rho K \sum_{m=1}^{M} \left(V_m^* \Gamma_m \cos\beta_{i\,m} - (1/2) V_m^{*\,2} l_m C_{D\,m} \sin\beta_{i\,m} \right) \Delta r_m$$

$$Q = \rho K \sum_{m=1}^{M} \left(V_m^* \Gamma_m \sin\beta_{i\,m} + (1/2) V_m^{*\,2} l_m C_{D\,m} \cos\beta_{i\,m} \right) r_m \Delta r_m \qquad (20)$$

where Δr_m is the radial distance between the two lattice points surrounding the control point m, K is the number of blades and M the number of control points. V_m multiplied by the sine/cosine represents the axial/tangential components of the velocity field which in turn is composed of the inflow and the velocities induced by the lifting lines.

The induced axial velocity u_m and induced tangential velocity v_m can be expressed as

$$u_m = \sum_{n=1}^{M} \Gamma_n u_{m,n}^* \qquad v_m = \sum_{n=1}^{M} \Gamma_n v_{m,n}^* \qquad (21)$$

where $u_{m,n}^*$ is the summation of the axial velocity induced at the control point m by a horseshoe vortex of unit strength surrounding the control point n in the absence of a duct plus the axial velocity induced by the duct in the presence of such a vortex at the same point m. The same definition stands for $v_{m,n}$ substituting the word *axial* by *tangential*.

In our variational approach the thrust generated by the duct is computed but its effect on the optimum circulation distribution is not included. We form the quantity $H=Q+\lambda T_P$ which is to be minimized. The Lagrange multiplier, λ, is to be solved along with the Γ_m's. Expanding H and setting its partial derivatives with respect to the Γ_m's equal to zero, gives us M equations for the M discrete values of circulation and the Lagrange multiplier. An additional equation is provided by specifying the required thrust in (20).

The distribution of thrust between the propeller and the duct is determined in an iterative way. In the first iteration we enter equations (21) and (20) with T_P equal to T_T and we solve for the Γ_i's. Then we compute the T_D which is a quadratic function of the Γ_i's. The new T_P is now calculated as the difference between T_T and T_D. This process is repeated until convergence is obtained.

The hub thrust has not been considered as pointed out in Section 2.3.

2.4.3 INCLUSION OF THE DUCT AND HUB SURFACES

In order to consider the influence of the duct and hub surfaces in the lifting line code we have to account in the optimization scheme not only for the components of the velocity $\mathbf{U}_{inflow}$ and $\mathbf{q}_{LL}$ as in a conventional code but also for the additional terms $\mathbf{q}_0(l)$ and $\Gamma_i \mathbf{q}_i(l)$ (see equation (7)). The vector $\mathbf{q}_0$ has only axial and radial components and only the first one should be added to the axial component of the inflow because the radial component is not included in the optimization scheme of a conventional propeller. The vector $\mathbf{q}_i$ has three components, and only the tangential and axial ones will be considered in the variational optimization.

2.4.4 CHORDLENGTH SELECTION

The chordlengths are usually selected by cavitation considerations and they are determinant in the distribution of viscous forces along the propeller blade. Since the local cavitation number is a function of the induced velocity, which in turn depends on the circulation distribution, the chordlengths are selected as a part of the circulation optimization procedure.

Employing the same procedure developed in Ref. 2, the chord shape is defined by a third order b-spline, as described by Roger and Adams (Ref.17), with either four or five vertices. The vertices are chosen so that the resulting chordlengths vary from the input hub chordlength to zero at the tip. The chordlengths are further required to be everywhere greater than the minimum chordlength from the cavitation considerations described below. The use of b-splines insures a smooth curve defined by a few points only.

The foil section is assumed to be a NACA 66 (TBM modified nose tail) profile with a NACA a=0.8 meanline. Brockett (Ref. 18) presents a figure showing the optimum geometry for a given minimum pressure coefficient for this section. Kroeger (Ref. 19) mapped this figure to the following equation:

$$\sigma(r) = 26.67 \left(\frac{c(r)}{l(r)}\right)^2 + 8.09 \left(\frac{c(r)}{l(r)}\right) + 10.0 \left(\frac{c(r)t(r)}{l(r)l(r)}\right) + 3.033 \left(\frac{t(r)}{l(r)}\right) \qquad (22)$$

where $c(r)$ is the camber distribution, $l(r)$ is the chord distribution, $t(r)$ is the thickness distribution and $\sigma(r)$ is the local cavitation number. Solving for the chord distribution we have:

$$l(r) = \frac{(8.09c(r) + 3.033t(r))}{2\sigma(r)} + \frac{\sqrt{(8.09c(r) + 3.033t(r))^2 + 4\sigma(r)(26.67c^2(r) + 10c(r)t(r))}}{2\sigma(r)} \qquad (23)$$

With linearized, ideal, two-dimensional camber we have:

$$c(r) = \frac{2\pi}{\kappa} DG(r) \frac{V_s}{V^*} \qquad (24)$$

where: κ = 15.035 for this foil section.

For small cavitation numbers, $\sigma(r)<0.54$, $l(r)$ from equation (24) is used as the minimum chordlength. For intermediate cavitation numbers, $0.54<\sigma(r)<1.16$, the chord is further required to be greater than five times the local thickness.

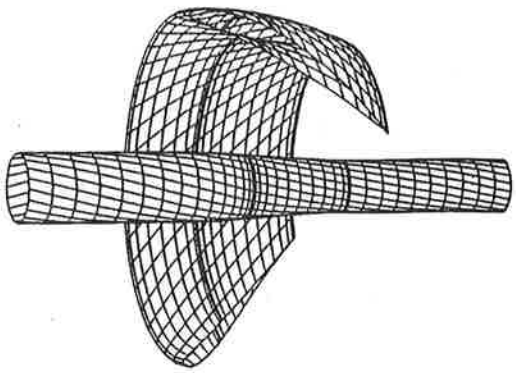

Figure 4: Panel arrangement on the duct and hub. For the duct 40 chordwise and 40 circumferential panels were used and half of them are shown. For the hub 37 longitudinal and 20 circumferential panels were used. *Half-cosine spacing* was chosen for the 15 strips located upstream from the lifting line, *cosine spacing* for the 12 located between the plane of the lifting lines and that of the duct trailing edge, and *constant spacing* for the 10 located downstream from the duct trailing edge.

3. IMPLEMENTATION

3.1 GEOMETRY AND GRID GENERATION

Duct

The duct is defined as an axisymmetric surface with a constant meridional section. The parameters which determine its geometry are: the chordlength, the radius at the nose of the duct, the camber and thickness of the duct section, and the angle between the nose-tail line and the axis of rotation.

The grid on the duct in the axial direction is divided into two regions which are defined by the duct edges and the plane of the lifting line. Cosine spacing is used for the longitudinal panelling inside each one of those regions in order to achieve a greater resolution near the lifting lines and duct edges. The circumferential panelling has a constant angular step and the grid follows a helical pattern. Figure 4 shows half the grid of the duct for an arrangement of 40 circumferential and 40 chordwise panels together with the grid of the hub. The grid of the wake has also been panelled but it is not shown in this figure.

Hub

The hub is modelled as an axisymmetric surface divided into three parts: two straight cylinders which represent the upstream hub surface and the hub vortex, and an intermediate surface with a radius which varies longitudinally according to a third degree polynomial tangent to both cylinders. This hub model, which in principle is extended from infinity upstream to infinity downstream, is made finite in order to make it possible to implement it in the computer code. The hub is therefore cut at a distance upstream and downstream from the lifting line location.

The parameters which define its geometry are: the length of the hub upstream and downstream of the propeller lifting lines, the upstream hub radius, the hub vortex radius and the longitudinal location of the upstream and downstream edges of

Figure 5: Panel arrangement on the hub for 30 longitudinal and 20 circumferential panels. Constant spacing was used.
plane.

the intermediate region.

The longitudinal panelling on the hub is of three types, as shown in Figure 4: *half-cosine spacing* upstream of the lifting line plane, with the fine spacing near the lifting lines; *cosine spacing* in the region between the plane of the propeller lifting lines and that of the duct trailing edge, matching the grid of the duct in that region; and *constant spacing* downstream of the duct trailing edge, matching the spacing of the panels at the wake of the duct.

In the case of a lifting line model with hub and no duct the axial spacing is constant along the hub, as shown in Figure 5. The circumferential panelling is formed from constant angular increments, matching those on the duct grid at the propeller

Wake

The grid in the wake is generated according to the theory of lightly loaded propellers following a helical pattern of constant pitch. However the computer code allows a pitch at the hub different from that at the duct. The wake is aligned with the undisturbed relative inflow at each radial location and therefore its geometry can be determined in terms of the advance coefficient J.

A moderately loaded theory would require that the wake be aligned with the induced flow at the lifting line. This would result in an iterative process in which the duct, hub, and wake surfaces should be repanelled at each step according to an updated radial varying pitch. The pitch in this case would be determined not only by the axial and tangential components of the inflow (U_{inflow}) but also by the three perturbation velocity components q_{LL}, q_i, and q_0, according to equation (7). This procedure, however, would take excessive CPU time to run on the computer since influence coefficients must be evaluated in each iteration.

3.2 CONVERGENCE TESTS

3.2.1. Pressure Tests

Hub in Axisymmetric Flow

Two different hubs with identical geometry but different lengths were tested. The geometrical data relative to the length of the intermediate region of the hub are:

* upstream radius 0.20 and downstream radius 0.15
* intermediate region extended from x=0 to x=1
* total length of the hubs 3.00 (from x=-1.00 to x=2.00) and 4.00 (from x=-1.50 to x=2.50).

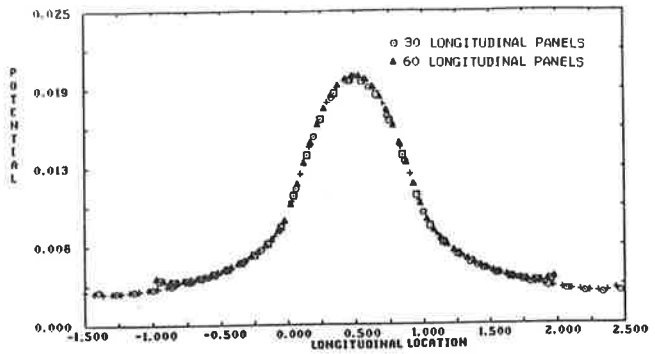

Figure 6: Potential distribution for two hubs in axisymmetric flow. The geometry is described in section 3.2.1. For each hub two discretizations were used: 20 circumferential by 30 longitudinal panels and 40 circumferential by 60 longitudinal panels.

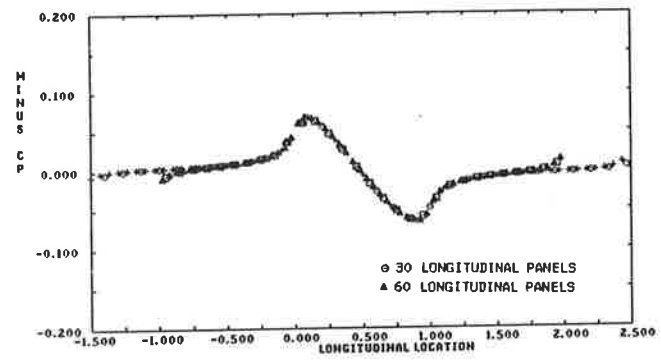

Figure 7: Pressure distributions derived from the potentials shown in Figure 6, for the same panellings.

For each length, two different panellings were considered: 20 circumferential by 30 axial panels and 40 circumferential by 60 axial panels. The geometry of the shorter hub with the first panelling is given in Figure 5.

From Figures 6 and 7 where the results for potential and pressure distributions are displayed, it can be seen that convergence is obtained with a relatively small number of panels. Only at the edges of the hub are there small variations in both distributions from the correct value of zero, that is expected. These differences are due to the fact that our hub model is finite and near the hub edges we can expect a flow slightly different from that in the case of an infinite hub. The flow at the hub edges will converge to that of an infinite hub as the length of the hub model is increased upstream and downstream from the intermediate region. This is illustrated in Figure 7: the longer hub has more uniform potential distribution at the edges. In any event, the potential converges very fast in the neighbourhood of the lifting line location which is our region of interest.

Duct in Axisymmetric Flow

The geometrical data of the duct tested are as follows:

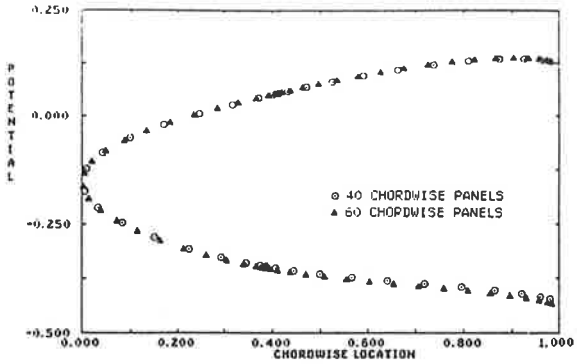

Figure 8: Potential distribution for a duct in axisymmetric flow. Two panellings with 40 circumferential by 40 chordwise panels and 60 circumferential by 60 chordwise panels were used.

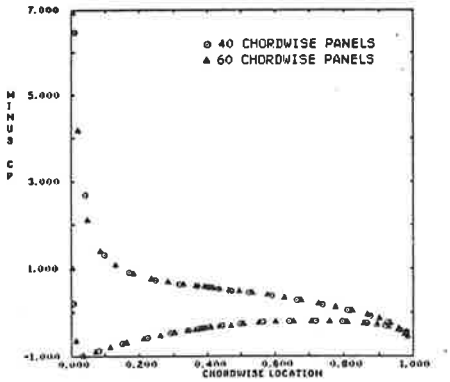

Figure 9: Pressure distribution derived from the potentials given in Figure 8.

* camber ratio *f/c*, 0.00
* thickness ratio *t/c*, 0.15
* nose-tail angle in the duct section 10.2 deg
* ratio of the radius at the nose to the chord, 1.00

The geometry of the duct tested is the same as that in Figure 4. To decrease the influence of the vorticity generated in the end-wake region of the duct, on the velocity field near the propeller, the length of the wake is made five duct-chordlengths long. The potential and pressure distribution for 40x40 and 60x60 panels are shown in Figures 8 and 9 respectively. The size of the panels on the duct is larger than that on the hub, therefore convergence is obtained with a greater number of panels.

Duct and Hub in Axisymmetric Flow

The geometry of the duct and hub tested is shown in Figure 4 and has been described in this section.

To decrease the influence of the end-wake region of the duct on the velocity field near the propeller, the length of the wake is made five duct-chordlengths long as in the previous section. The hub vortex and the lifting line wakes were extended the same distance.

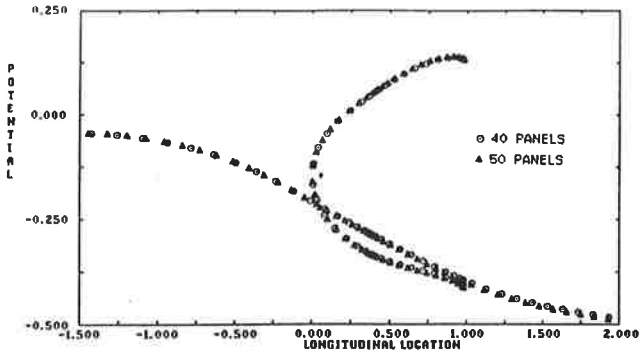

Figure 10: Potential distribution for duct and hub in axisymmetric flow. The curve within the interval (0,1) represents the potential on the duct and that extended from -1.5 to 2 represents the potential on the hub. A jump at the duct trailing edge can be observed. Two panellings were used with the following circumferential by longitudinal numbers of panels: the first, with 40x40 on the duct and 40x40 on the hub; the second, with 50x50 on the duct and 50x50 on the hub.

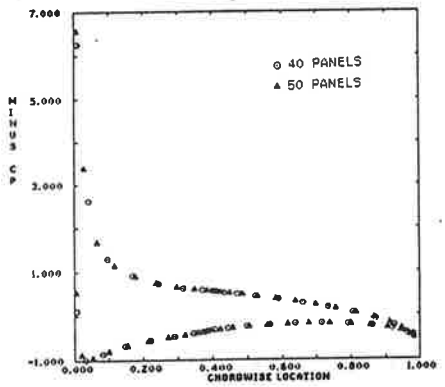

Figure 11: Pressure distribution derived from the duct potential in Figure 10.

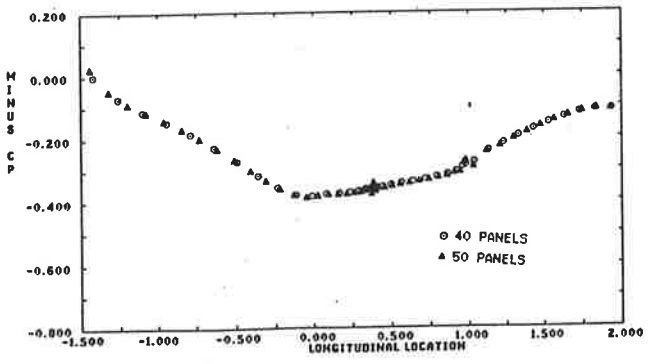

Figure 12: Pressure distribution derived from the hub potential in Figure 10.

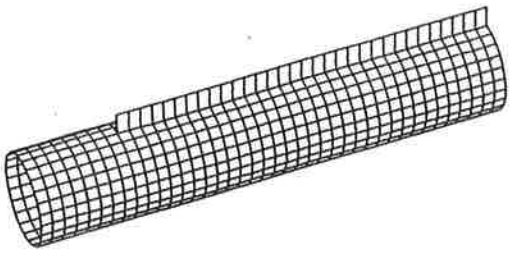

Figure 13: Horseshoe set on straight cylinder. The pitch angle for the trailing vorticity is 90 deg. For this figure 25 circumferential and 40 longitudinal panels were used on the cylinder.

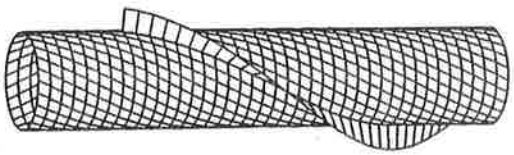

Figure 14: Horseshoe set on straight cylinder. The pitch angle for the trailing vorticity is 80 deg. For this figure 25 circumferential and 40 longitudinal panels were used on the cylinder.

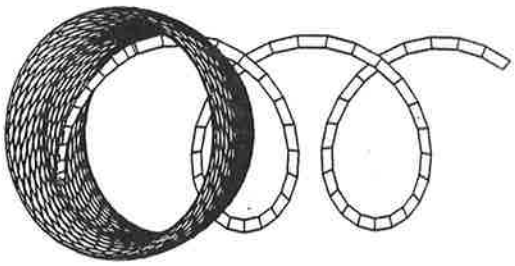

Figure 15: Horseshoe set on the inner surface of the duct. The pitch angle for the trailing vorticity is 23 deg. For this figure 40 circumferential and 40 chordwise panels were used on the duct.

VELOCITIES ON LIFTING LINE DUE TO A HORSESHOE INSIDE A DUCT
(NONDIMENSIONAL ON U = SHIP SPEED)

HORSESHOE INNER RADIUS/ RPROP : 0.2000000
HORSESHOE OUTER RADIUS/ RPROP : 0.3000000
HORSESHOE STRENGTH G/2/PI/U/RPROP : 5.0000001E-02
NUMBER OF AXIAL PANELS ON HUB : 40
NCP: NUMBER OF CIRCUMFERENTIAL PANELS

HORSESHOE PITCH ANGLE (DEGRS): 90.00000

NCP	R	VELX	VELR	VELTH
20	0.250000	-0.000005	0.000000	0.281750
25	0.250000	-0.000004	0.000000	0.285210
IMAGE METHOD:	0.250000	0.000000	0.000000	0.285714

ALFA: ANGLE BETWEEN TOTAL VELOCITY AND A PLANE PERPENDICULAR TO THE HUB
HORSESHOE PITCH ANGLE (DEGRS): 80.09973

NCP	TAN(ALFA)	VELX	VELR	VELTH	VELTOT
20	0.171771	-0.047050	0.016839	0.273911	0.278432
25	0.174442	-0.048365	0.019810	0.277256	0.282139
IMAGE METHOD:	0.174533				0.285714

Table I: Comparison between the velocity field computed by a panel method and that predicted by an image vortex calculation. A horseshoe acting in the presence of a straight cylinder is studied. The control point is located at the middle of the horseshoe bound segment. Two pitch angles for the horseshoe trailing vorticity are considered, 90 and 80 deg. The length of the cylinder is twelve and a half times the cylinder diameter.

To reduce the number of control points on the hub surface, only control points between the duct trailing edge and one duct chordlength downstream were considered on the hub vortex surface. However, the influence of more distant panels along this surface was taken into account at each control point. This was accomplished by assuming that the potential remains constant for all those distant panels located on the same helical strip. The value of the potential for the distant panels along each strip was set equal to the value of the potential at the nearest panel having a control point in the same strip.

The distributions of the potential on hub and duct, pressures on the hub and pressures on the duct are shown in Figures 10, 11, and 12 respectively for two different panellings. In the last figure the pressure coefficient C_p tends to zero at both hub edges located at x=-1.5 and x=6. The downstream edge of the hub does not appear in the plot since no control point has been set on this region; however the tendency is observed in the dowstream control points.

3.2.2 VELOCITY TEST

Two tests were performed in order to check the accuracy of the panel method for predicting the velocity field at the lifting line plane before solving the final problem: flow around a hub, due to horseshoes set on its surface (see Figures 13 and 14); and flow around a duct, due to a horseshoe set on its inner surface (see Figure 15). The control point in both cases was located in the middle of the bound segment of the horseshoe.

In the first test the hub was modelled as a straight cylinder and the induced velocity was calculated at the control point for two pitch angles in the horseshoe trailing vorticity, 90 and 80 deg. These results were compared with the values obtained by an image vortex calculation. The image method has been chosen to check the panel method predictions since it is very accurate for predicting the velocity field, especially in

VELOCITIES ON LIFTING LINE DUE TO A HORSESHOE INSIDE A DUCT
(NONDIMENSIONAL ON U = SHIP SPEED)

HORSESHOE INNER RADIUS/ RPROP : 0.9212205
HORSESHOE OUTER RADIUS/ RPROP : 1.000000
HORSESHOE STRENGTH G/2/PI/U/RPROP : 5.0000001E-02
HORSESHOE PITCH ANGLE BETAI (DEGRS): 23.03288

GRID ON THE DUCT

NUMBER OF CHORWISE PANELS ON DUCT : 80
NUMBER OF CIRCUMFERENTIAL PANELS : 80
NUMBER OF BLADES : 5

X	R	VELX	VELR	VELTH
0.380524	0.251595	0.033501	0.002262	-0.000046
0.380524	0.330374	0.034084	0.003024	-0.000136
0.380524	0.409154	0.034818	0.003750	-0.000313
0.380524	0.487933	0.035638	0.004313	-0.000601
0.380524	0.566713	0.036307	0.004452	-0.000989
0.380524	0.645492	0.036099	0.003672	-0.001346
0.380524	0.724272	0.032897	0.001108	-0.001236
0.380524	0.803051	0.020093	-0.004710	0.000665
0.380524	0.881831	-0.029522	-0.016505	0.009740
0.380524	0.960610	-0.402104	0.007663	0.104356

VELOCITIES ON LIFTING LINE DUE TO A HORSESHOE INSIDE A DUCT
(NONDIMENSIONAL ON U = SHIP SPEED)

HORSESHOE INNER RADIUS/ RPROP : 0.9212205
HORSESHOE OUTER RADIUS/ RPROP : 1.000000
HORSESHOE STRENGTH G/2/PI/U/RPROP : 5.0000001E-02
HORSESHOE PITCH ANGLE BETAI (DEGRS): 23.03288

GRID ON THE DUCT

NUMBER OF CHORWISE PANELS ON DUCT : 100
NUMBER OF CIRCUMFERENTIAL PANELS : 100
NUMBER OF BLADES : 5

X	R	VELX	VELR	VELTH
0.380524	0.251595	0.034103	0.002237	-0.000046
0.380524	0.330374	0.034695	0.002991	-0.000136
0.380524	0.409154	0.035441	0.003709	-0.000313
0.380524	0.487933	0.036276	0.004265	-0.000602
0.380524	0.566713	0.036963	0.004399	-0.000991
0.380524	0.645492	0.036780	0.003619	-0.001354
0.380524	0.724272	0.033617	0.001060	-0.001264
0.380524	0.803051	0.020916	-0.004779	0.000571
0.380524	0.881831	-0.028383	-0.016935	0.009303
0.380524	0.960610	-0.392181	-0.013301	0.092248

Table II: Velocity induced by a horseshoe set on the inner surface of the duct. Two panellings were used: 80 circumferential by 80 chordwise panels and 100 circumferential by 100 chordwise panels.

the case of a straight horseshoe close to a cylinder.

The image vortex was obtained in the following way: if r is the radius of the trailing vortex and β its pitch, the radius of the image, r_{image}, is given by

$$r_{image} = \frac{r_{hub}^2}{r}$$

where r_{hub} is the radius of the hub; and the pitch of the image, β_{image}, is given by

$$\tan(\beta)_{image} = \frac{r}{r_{image}} \tan(\beta)$$

Table I shows a comparison of the results obtained by both methods. Notice that three digits of accuracy are obtained for the tangential velocity with only 25 circumferential panels in the case of a straight horseshoe, and the same accuracy is obtained for the ratio of the axial velocity to the tangential velocity in the case of a horseshoe with a pitch angle of 80 deg.

The second and more difficult test was performed with the

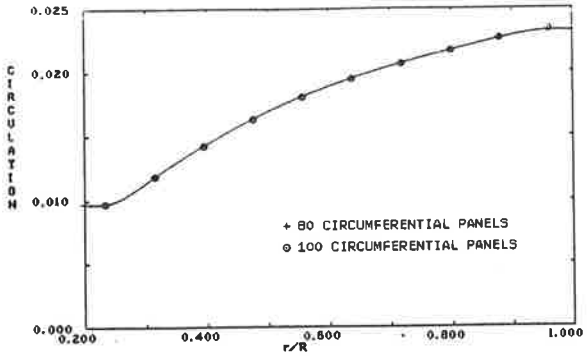

Figure 16: Optimum radial distribution of circulation for the ducted propeller with hub described in this section. No gap at the tip is allowed. J=1.1 and C_T=0.481. Two circumferential panellings on the duct and hub were considered with 80 and 100 panels. The number of control points is 10 in both cases. The non-dimensional circulation is given by $G=\Gamma/\pi DV$.

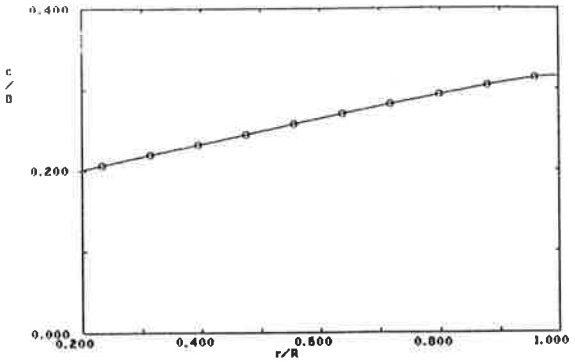

Figure 17: Radial distribution of chordlength for the ducted propeller with hub described in this section. J=1.1 and C_T= 0.481.

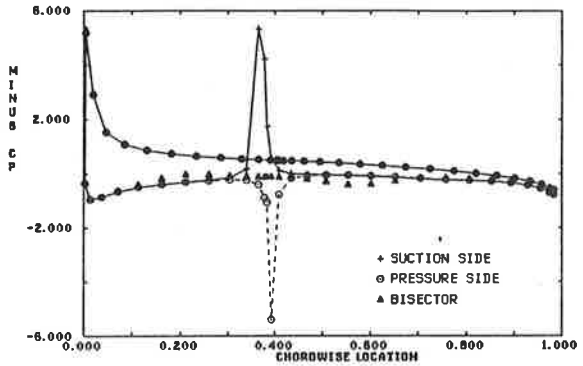

Figure 18: Pressure distribution on duct for the flow around a lifting line with duct and hub. Three helical strips on the duct were considered, the first close to the suction side of the lifting line, the second close to the pressure side, and the last following a bisector between blades. For this calculation 100 circumferential and 60 longitudinal panels were used.

actual duct geometry. The criterion used for the panel size was that the panel's main dimensions should be smaller than or approximately equal to one and a half times the distance d from the lifting line control point to the duct surface.

To check this criterion two panellings were used 80 circumferential by 80 chordwise panels and 100 circumferential by 100 chordwise panels. The panel length in the axial direction meets this criterion since cosine spacing has been used for the axial panelling with fine spacing near the lifting line. The panel width meets this criterion for 100 circumferential panels but not for 80. In the latter case the panel width was approximately $1.9d$

Table II shows a pronounced difference in the prediction of the radial velocity at the lifting line control point near the tip. However the tangential and axial velocities, which enter into the scheme for the optimization of circulation, are closer. We can expect two digits of accuracy in the velocity components for the finer panelling.

4. DISCUSSION OF RESULTS

The optimum load distribution and chordlengths for a five-blade propeller operating inside a duct with hub were determined. The input data were:

* duct geometry as described in 3.2.1, with a section chordlength of 0.58 the propeller diameter and with a meridional thickness form NSRDC modified NACA 66.
* hub geometry as described in 3.2.1 with a hub radius at the lifting line of 0.19 the propeller radius and a hub vortex diameter of 0.50 the upstream diameter of the hub
* propeller diameter, 10 ft
* the propeller lifting lines are located at a distance from the duct nose of 0.40 times the duct length
* the advance coefficient J was fixed at 1.1
* the propeller thrust coefficient C_T was 0.481
* no gap between duct and lifting line was considered.

The duct was represented by 60 chordwise and 100 circumferential panels, the hub by 80 longitudinal and 100 circumferential panels, and the propeller by 10 horseshoes.

In order to reduce the total number of longitudinal unknowns on the duct and hub to 100, only 40 circumferential strips on the hub have control points. If we focus on a helical strip of panels on the hub, only the 40 panels located upstream have control points. The potential on the 40 remaining panels was considered to be the same as that at the last axial panel with control point. The number of circumferential unknowns was 20 because of between-blade symmetry. The total number of unknowns was therefore 2,000.

Figure 16 shows the optimized radial distributions of circulation with almost identical results for 80 and 100 circumferential panels on the duct-hub grid. Note that the circulation has a nonzero value at both ends of the lifting line. At one end the circulation is transferred to the hub and shed as a hub vortex. At the other end the circulation is transferred to the duct and therefore is not shed as a tip vortex.

Figure 17 shows the radial distribution of chordlength. The length of the root chord was required to be at least twenty

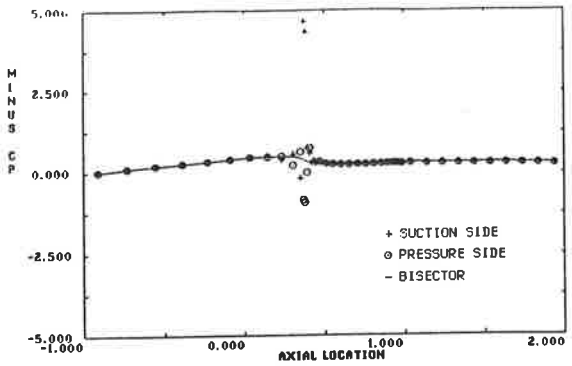

Figure 19: Pressure distribution on hub for the flow around a lifting line with duct and hub. Three helical strips on the hub were considered, the first close to the suction side of the lifting line, the second close to the pressure side, and the last following a bisector. For this calculation 100 circumferential and 40 longitudinal panels were used.

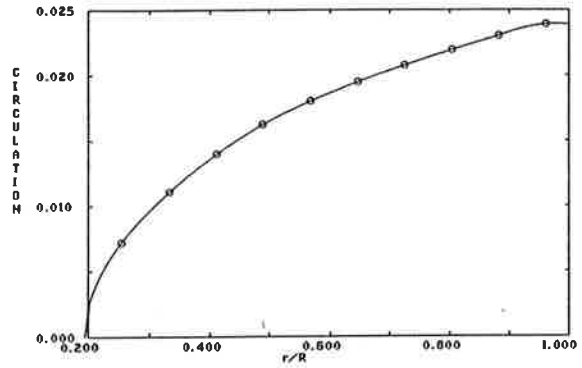

Figure 20: Optimum radial distribution of circulation for a ducted propeller without hub. No gap at the tip is allowed. J=1.1 and C_T=0.478. The non-dimensional circulation is given by $G=\Gamma/\pi DV$.

percent of the propeller diameter.

Figures 18 and 19 show the pressure distribution on hub and duct respectively. Of course, the pressure in the near field of the lifting line is unrealistic.

The computer code also allows us to handle the lifting line model with either hub or duct independently.

The optimum distribution of circulation for lifting lines operating inside a duct with no hub is given in Figure 20. The grid has 100 chordwise and 100 circumferential panels. The geometry for this arrangement is the same as the geometry for the previous arrangement in which a hub was present. Notice that the circulation falls to zero at the inner edge of the lifting line and attains a maximum value at the duct. A comparison of Figure 16 with Figure 20 shows that the presence of the hub has minimal influence on the maximum value of circulation.

Figure 21 shows the chordlength distribution for this arrangement. Notice that the ratio of the local chordlength to

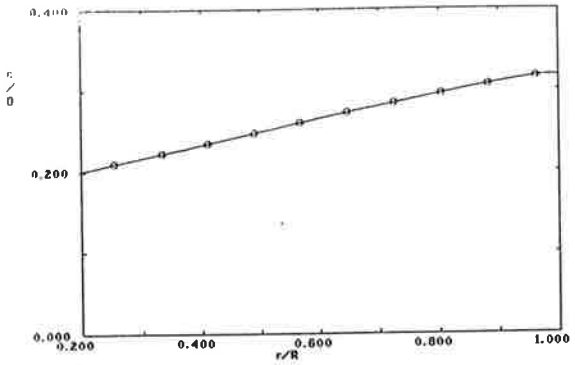

Figure 21: Radial distribution of chordlength for a ducted propeller without hub. J=1.1 and C_T= 0.478.

the propeller diameter is required to be at least 0.2 at the blade root.

A comparison between Figures 17 and 21 shows that the presence of the hub has minimal influence on the chordlength distribution.

The same distributions for an arrangement of lifting lines with hub but with no duct were computed. The grid had 80 axial and 60 circumferential panels. The geometry was the same as that already described in this section.

Figure 22 shows the optimum radial distribution of circulation for this arrangement from which it can be seen that the circulation falls to zero at the tip of the lifting line and has a nonzero value at the hub.

Figure 23 shows the chordlength distribution. Note that the chordlength at the blade root is again 0.2 times the propeller diameter, and at the blade tip the local chordlength falls to zero.

5. CONCLUSIONS

A lifting line representation of a propeller has been combined with a panel method representation of the duct and hub.

The convergence of the potential and pressure distributions on the hub and duct surfaces has been investigated first in axisymmetric flow. Then, convergence of the velocity field due to non-axisymmetric interactions between either duct or hub and lifting lines has been studied. Finally, optimum distributions of circulation and chordlength have been obtained and presented for three cases:

* lifting lines operating inside a duct with hub
* lifting lines operating inside a duct with no hub
* lifting lines operating in the presence of a hub alone.

The presence of the hub was found to have minor influence on the maximum of the circulation for a ducted propeller. The presence of the duct was found to have little influence on the value of the circulation at the root of the blade.

The current theory allows for the design of a ducted propeller in which no gap is considered between the propeller tip and the duct. Following the conclusions presented by Kerwin, Kinnas, et al. [7], the results from the analysis of the

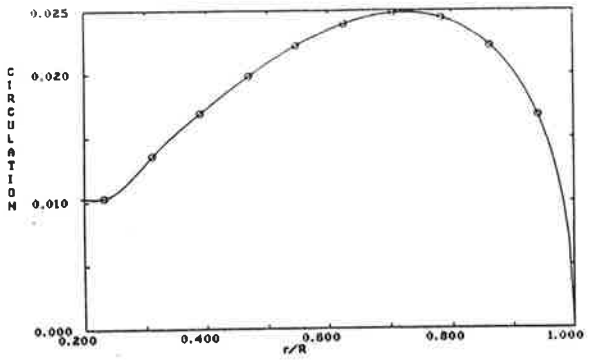

Figure 22: Optimum radial distribution of circulation for a conventional propeller modelled with hub. J=1.1 and C_T=0.480.

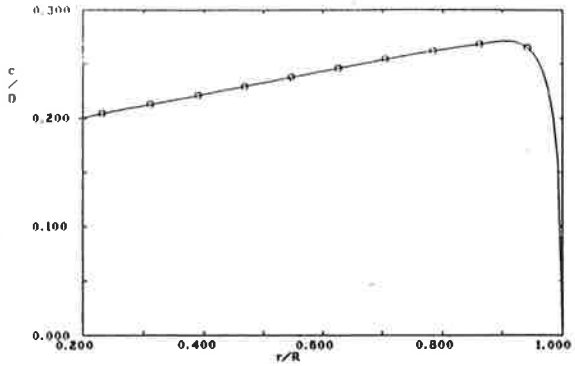

Figure 23: Radial distribution of chordlength for a conventional propeller modelled with hub. J=1.1 and C_T=0.480.

potential flow around a ducted propeller are physically meaningful for zero gap or large gap relative to the propeller radius. For intermediate gaps, the results are expected to be unrealistic since viscous effects dominate the flow in this region. A future extension of our design method could be to consider intermediate gaps by modelling the gap cross flow equation as suggested in [7].

ACKNOWLEDGEMENTS

The author wishes to thank the Propeller team of the Department of Ocean Engineering at M.I.T. for their support and valuable assistance. Especially, the author is greatly indebted to Professor J.E. Kerwin, S. Kinnas and B. Coney for the help they provided during this research.

REFERENCES

1 E.B. Caster. *A Computer Program for Use in Designing Ducted Propellers*. Technical Report 2507, NSRDC, 1967.

2 William B. Coney, Ching-Yeh Hsin, and Justin E. Kerwin. *A Vortex Lattice Lifting Line Program for Single and Multi-Component Propulsors MIT PLL-2 Report and User's Manual*. Technical Report, Department of Ocean Engineering, MIT, December 1986.

3 I.S. Gibson and R.I. Lewis. Ducted propeller analysis by surface vorticity and actuator disc theory. In *Proceedings of the Symposium on Ducted Propellers*, The Royal Institution of Naval Architects, Teddington, England, MAY 1973.

4 E.J. Glover and P.G. Ryan. A comparison of the theoretical and experimental perfomance of a ducted propeller system. In *Proceedings of the Symposium on Ducted Propellers*, The Royal Institution of Naval Architects, Teddington, England, MAY 1973.

5 S. Goldstein. On the vortex theory of screw propellers. In *Proceedings of the Royal Society*, pages pp.440-465, 1929.

6 J.L. Hess and Walter O. Valarezo. Calculation of steady flow about propellers by means of a surface panel method. In *23rd Aerospace Sciences Meeting*, AIAA, Reno, Nevada, January 1985.

7 J.E. Kerwin, S.A. Kinnas, J-T Lee, and W-Z Shih. A surface panel method for the hydrodynamic analysis of ducted propellers. *Trans. SNAME*, 95, 1987.

8 J.E. Kerwin and R. Leopold. A design theory for subcavitating propellers. *Trans. SNAME*, 1964.

9 Spyros A. Kinnas and William B. Coney. *On the Optimum Ducted Propeller Loading*. Technical Report, SNAME Propellers 88 Conference, September 1988.

10 Jin-Tae Lee. *Propeller Steady Flow Analysis Program Using a Potential Based Panel Method*. Technical Report, Department of Ocean Engineering, MIT, August 1987.

11 H.W. Lerbs. Moderately loaded propellers with a finite number of blades and an arbitrary distribution of circulation. SNAME, pp.13-14, Nov. 1952.

12 K. Ludolph. *Propeller-Hub Interference Effects Using an Approximate Lifting Surface Theory*. Technical Report, Applied Research Laboratory, The Pennsylvania State University, June 1977.

13 B.W. McCormick. The effect of a finite hub on the optimum propeller. *Journal of the Aeronautical Sciences*, 22(9), Sep. 1955.

14 Wang M.H. *Hub Effects in Propeller Design and Analysis*. Technical Report No 85-12, Department of Ocean Engineering, MIT, May 1985.

15 W.B. Morgan. Theory of the annular airfoil and ducted propeller. In *Fourth Symposium on Naval Hydrodynamics*, pages pp 151-197, 1962.

16 Luigi Morino and Ching-Chiang Kuo. Subsonic potential aerodynamic for complex configurations: a general theory. *AAIA J.*, vol 12(no 2): pp 191-197, February 1974.

17 Roger and Adams. *Mathematical Elements for Computer Graphics*,McGraw-Hill, 1976.

18 T. Brockett. *Minimum Pressure Envelopes for Modified* NACA-66 *Sections with* NACA *a*=0.8 *Camber and Buships Type I and Type II Sections*. Technical Report no 1780, DTNSRDC. Teddington, England Feb. 1966.

19 N.B.Kroeger. *Optimization of Propulsion Speeds*. Technical Report, Department of Ocean Engineering, MIT, June 1972.